The role of the permanent wilting point in controlling the spatial distribution of precipitation

Cathy Hohenegger[a,1] and Bjorn Stevens[a]

[a]Max Planck Institute for Meteorology, 20146 Hamburg, Germany

Edited by Kerry A. Emanuel, Massachusetts Institute of Technology, Cambridge, MA, and approved April 17, 2018 (received for review October 31, 2017)

Convection-permitting simulations on an idealized land planet are performed to understand whether soil moisture acts to support or impede the organization of convection. Initially, shallow circulations driven by differential radiative cooling induce a self-aggregation of the convection into a single band, as has become familiar from simulations over idealized sea surfaces. With time, however, the drying of the nonprecipitating region induces a reversal of the shallow circulation, drawing the flow at low levels from the precipitating to the nonprecipitating region. This causes the precipitating convection to move over the dry soils and reverses the polarity of the circulation. The precipitation replenishes these soils with moisture at the expense of the formerly wet soils which dry, until the process repeats itself. On longer timescales, this acts to homogenize the precipitation field. By analyzing the strength of the shallow circulations, the surface budget with its effects on the boundary layer properties, and the shape of the soil moisture resistance function, we demonstrate that the soil has to dry out significantly, for the here-tested resistance formulations below 15% of its water availability, to be able to alter the precipitation distribution. We expect such a process to broaden the distribution of precipitation over tropical land. This expectation is supported by observations which show that in drier years the monsoon rains move farther inland over Africa.

radiative convective equilibrium | ITCZ | soil moisture | precipitation | mesoscale circulation

The vertical temperature structure of the tropical climate (1) as well as its mean state (2) can be understood in terms of a much simpler analogue, radiative convective equilibrium (RCE). In RCE, the Earth does not rotate and is covered by water, the insolation is spatially homogeneous, and the heat transport is governed by the two atmospheric processes radiation and convection. Radiation acts to destabilize the atmosphere and convection to stabilize it. In RCE, also, the convection tends to self-aggregate into larger-scale structures (2–6), often through the generation of radiatively driven circulations of depth much shallower than the convection itself (6). To what extent the processes responsible for the self-aggregation of convection influence large-scale convective structures observed over tropical oceans, such as the intertropical convergence zone (ITCZ), remains an open and hotly debated topic (7–10).

In this simple analogue, the atmosphere has access to an infinite supply of moisture from the oceanic surface. In contrast, over land, the local supply of moisture is finite and the land can dry out. What is the effect on the precipitation distribution of a variable and possibly limited supply of moisture from the surface to the atmosphere? Is the fundamental role of soil moisture to maintain precipitation in the precipitating region or to bring it to the nonprecipitating region? Here we answer this question using the RCE framework applied to a land-like setup that retains only the primary effects of soil moisture on the atmosphere.

Although the link between soil moisture and precipitation has long been studied, it remains strongly debated. One source of discrepancy is that the response of convective precipitation to soil moisture perturbation, as obtained in models using convective parameterizations such as global climate models, is inconsistent with the response obtained in observations (11) or in models using explicit convection (12). A second challenge is to actually adequately determine soil moisture effects (13, 14), as the latter are blurred by synoptic variability and by the complex structure of the Earth's surface. Three recent studies have used the simpler RCE framework to study aspects of the land climate, namely the enhancement of precipitation over islands (15), the land–ocean warming contrast (16), and potential equilibria of the land–atmosphere system in a one-column model version (17). The results of these studies suggest that there might be something to be learned from the simpler RCE framework.

Physically, the ability of soil moisture to store water and lose water in interaction with the atmosphere affects the partitioning between sensible and latent heat flux and through this the precipitation distribution in two potentially opposing ways. First, a change in the Bowen ratio affects the stability of the atmosphere and hence the triggering of convection. The most common response is that an increase in soil moisture favors the triggering of convection (18, 19) and hence increases precipitation. Following this argument, soil moisture maintains precipitation in the precipitating region. Second, the spatially localized nature of convective precipitation leads to the development of soil moisture gradients. Gradients in soil moisture lead to gradients in sensible heat flux, which can thermally induce a shallow circulation with surface flow from the wet to the dry region. This circulation can lead to the triggering of convection over the dry region (20, 21), a phenomenon that has been in particular observed in the Sahel region (22), although its signature has been

Significance

One basic distinction between land and ocean is that the land can dry out. We show that this is of fundamental importance for the precipitation distribution over land as it brings precipitation from the precipitating region to the nonprecipitating region. This process prevents the land–atmosphere system from sustaining precipitation over the same region and thus acts against drought or the formation of desert. Paradoxically, although dry atmospheres are known to hamper moist convection, drying the soil to its permanent wilting point generates circulations that are strong enough to overcome this inhibition. Our findings help understand why tropical rain bands broaden poleward over land, the more so the drier the soils are.

Author contributions: C.H. and B.S. designed research; C.H. conducted simulations; C.H. analyzed data; and C.H. wrote the paper with input from B.S.

The authors declare no conflict of interest.

This article is a PNAS Direct Submission.

Data deposition: Primary data and scripts used in this paper can be downloaded at https://powerfolder.gwdg.de/dl/fi5rX8X6VpnsqxZAcVr25qaD/.zip.

[1]To whom correspondence should be addressed. Email: cathy.hohenegger@mpimet.mpg.de.

This article contains supporting information online at www.pnas.org/lookup/suppl/doi:10.1073/pnas.1718842115/-/DCSupplemental.

Published online May 14, 2018.

deciphered globally (23). Following this second argument, soil moisture brings precipitation to the nonprecipitating region.

Which of these two effects ends up controlling the spatial distribution of precipitation? Another effect that can modulate the precipitation response to soil moisture perturbation, not explicitly considered in our two previous arguments, is the presence of a background wind or of a large-scale circulation. Using an idealized setup similar to RCE but where atmospheric and soil profiles were relaxed back to reference profiles over daily and multidaily timescales, a recent study (24) obtained both random and more clustered precipitation distributions—depending on the presence or absence of an imposed background wind. This contrast occurred because convective triggering is favored over dry soils, but propagating convective clusters are enhanced over wet soils. In our RCE framework, no background wind is imposed, but the atmosphere allows the convection to self-aggregate into one cluster and develop its own circulation. Will the convection end up more or less aggregated? In this study, we quantify the feedbacks among convection, circulations, and soil moisture to answer this question.

Soil Moisture Brings Precipitation to the Nonprecipitating Region

We use a simple formulation for the land surface in our simulations, a formulation that retains the two key characteristics of soil moisture (*Materials and Methods*): its spatial and temporal variability through the action of precipitation and evaporation as well as its nonlinear control on the surface fluxes via the use of a resistance formulation (Eq. **5**). This model version is compared with a version where the soil moisture resistance is set to zero, mimicking the situation of an infinite supply of water.

In our simulations, convection rapidly develops and produces precipitation with a daily mean of around 4.6 mm·d^{-1}. The spatial distribution of precipitation (Fig. 1) indicates that in both model versions convection organizes as time proceeds. That convection spontaneously begins to self-aggregate into a large convective structure is a well-known feature from past RCE simulations, as noted previously. Interactive soil moisture leads to little difference between the simulations up to around day 60. The monthly mean precipitating area, calculated from days 25 to 55, occupies 76% of the domain in both simulations. Hence, during this time period, the precipitation distribution is fully controlled by the atmosphere. This is consistent with values of the atmospheric resistance r_a that are much larger than values of the soil moisture resistance r_s, for instance 100 times larger at noon.

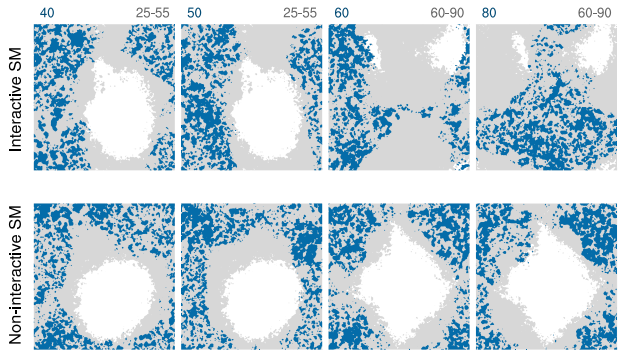

Fig. 1. Selected daily (blue shading) overlaid on monthly (gray shading) precipitating area for simulations with and without interactive soil moisture. The precipitating area is defined as the area where the surface precipitation mixing ratio accumulated over the chosen time period exceeds 0.1 g·kg^{-1} (about 4 mm of rain). The selected days are days 40, 50, 60, and 80, whereas the selected months are days 25–55 (two *Left* plots), before soil moisture becomes important, and days 60–90 (two *Right* plots).

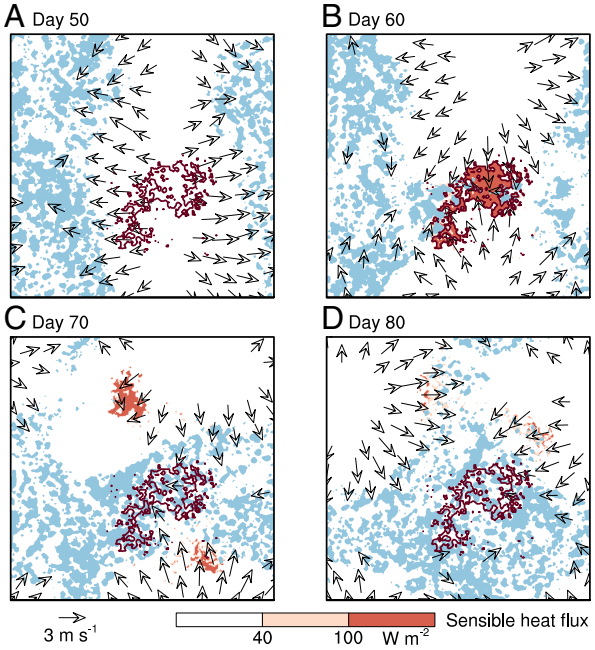

Fig. 2. Spatial interplay between wind (arrows, lowest model layer at 37.5 m), the precipitating area (blue shading, defined in Fig. 1), and sensible heat flux (red shading as shown in the color bar) averaged on days 50 (*A*), 60 (*B*), 70 (*C*), and 80 (*D*). The dark red contours, referred to as the desiccated region, enclose all the points where the soil moisture reaches its permanent wilting point on day 60. Only wind vectors with velocity larger than 2 m·s^{-1} are plotted.

The situation changes around day 60 (Fig. 1). Only in the simulation with interactive soil moisture, the precipitation begins to fall over the previously nonprecipitating area. The daily extent of the precipitating area remains similar in both simulations, but the location of the rainy points changes more rapidly with time when the soil moisture is coupled to the atmosphere; compare day 60 to day 80 in Fig. 1. The resulting homogenization of the precipitation field is clearly visible on a monthly timescale. Over days 60–90, the nonprecipitating area is reduced by a factor 3, from 29% down to 9% (gray shading in Fig. 1).

The Spatial Distribution of Precipitation Is Fully Determined by Shallow Circulations

We investigate the processes determining the spatial distribution of precipitation, in particular those leading to its homogenization by soil moisture. We focus on the simulation with interactive soil moisture around day 60.

The self-aggregation of convection, before day 60, is due to a shallow circulation (Fig. 2*A*) that spins up in the boundary layer due to the distinct radiative heating profiles of the nonprecipitating and the precipitating region: The former region is dry and at best populated by shallow convection, whereas the latter region is wet and populated by deep convection. The existence of such a circulation and its role for the self-aggregation of convection have been extensively demonstrated in previous convection-permitting RCE simulations using fixed sea surface temperature (SST) (e.g., ref. 6) and studied using a conceptual model (25). As in those past studies, horizontally homogenizing the radiative fluxes at each time step prevents the self-aggregation of convection. Key to note is that the surface component of the circulation is directed from the region of strong radiative cooling, the nonprecipitating area, to the region of weak radiative cooling, the precipitating area (Fig. 2*A*), and that its strength is a few meters per second. Given its genesis mechanism, we refer to this circulation as the radiatively driven circulation.

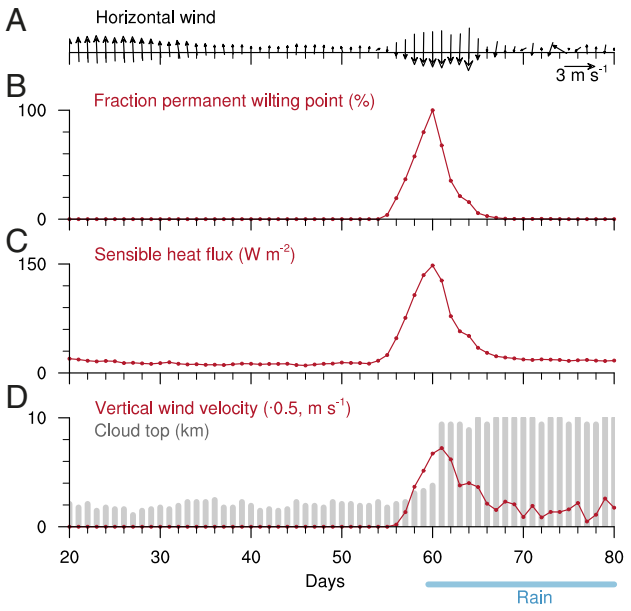

Fig. 3. Temporal interplay between wind, dryness, surface flux, and convective development for the desiccated region (defined in Fig. 2). Shown are time series of (*A*) the horizontal wind vector (37.5 m above ground) at a random grid point located on the northern boundary of the desiccated region, (*B*) the percentage of the region that is at its permanent wilting point, (*C*) the sensible heat flux, and (*D*) the vertical wind velocity (maximum value below 2 km, red line) and cloud top (gray bars). Quantities in *C* and *D* are averaged over the desiccated region. The cloud top is computed as the height where the region-averaged liquid water content drops below 0.005 g·kg^{-1}. The horizontal blue bar indicates when precipitation falls over the desiccated region.

The circulation maintains the convection aggregated in one band with minimal changes in direction (Fig. 3*A*). Around day 60, however, the circulation pattern drastically changes and begins to converge into the previously nonprecipitating region (Figs. 2*B* and 3*A*), called the desiccated region. The surface component of the circulation is now directed from the region of low sensible heat flux, the precipitating area, to the region of high sensible heat flux, the nonprecipitating area, with return flow at the top of the boundary layer. High sensible heat flux values are recorded once the soil moisture reaches its permanent wilting point, where bare soil evaporation shuts down. The agreement between permanent wilting point and enhanced sensible heat flux as well as circulation direction, in terms of spatial pattern (Fig. 2*B*) and temporal evolution (Fig. 3), indicates that the soil moisture gradient generates a thermally induced shallow circulation that is strong enough to alter the radiatively driven circulation.

Following the altered circulation pattern, precipitation starts falling on the desiccated region of the domain around day 60 (Figs. 2 and 3) and the two circulation forcings work hand in hand. As the precipitation replenishes the soil moisture, the surface forcing disappears in less than 10 d (Figs. 2 *B* and *C* and 3*C*). The radiatively driven circulation nevertheless maintains the new precipitation distribution until dry enough areas form in other parts of the domain and steal the precipitation (Fig. 2 *C* and *D*). This results in a permanent back and forth between the radiatively driven circulation, which wants to organize the convection in one place, and the soil moisture-induced circulation, which wants to disorganize the convection.

The above picture emphasizes the coupling between convection and circulations in determining the spatial distribution of precipitation. The circulation is very efficient at deepening the convection and producing precipitation, even in an otherwise unfavorable atmospheric environment. The atmosphere over the desiccated region is extremely dry on day 54, 1 d before the first grid points reach their permanent wilting point, with a water vapor path of 18.4 mm vs. 45.5 mm over the remaining domain. The relative humidity near the surface is only 60%, dropping to 13% above the low cloud tops (from 2 km to 6 km, Fig. 3*D*). Fig. 3*D* nonetheless indicates that it takes only 3 d for precipitation to start falling over the region once the soil moisture-induced circulation leads to ascent in the planetary boundary layer. As the circulation intensifies with more grid points reaching their permanent wilting point, the clouds deepen, abruptly reach 10 km on day 61, and produce similar precipitation amounts to those over other areas of the domain. In contrast, more than 50 d of continuous moistening by surface latent heat flux neither produces any significant precipitation nor produces any significant deepening of the cloud layer. The finding that direct moistening by surface latent heat flux is inefficient at triggering deep convection is consistent with studies that have looked at the diurnal evolution of deep convection in observations (26, 27). Likewise, under the action of sea breezes, convection has been observed to deepen in atmospheres that are much drier than over ocean (28). The tuning of convective parameterizations to be very sensitive to relative humidity, while global climate models are unable to resolve mesoscale circulations, distorts their ability to represent the distribution of precipitation over land, its controlling factors, and their susceptibility to change.

Does the Soil Need to Dry out?

To understand to which extent the soil needs to dry out to generate a circulation that is strong enough to alter the radiatively driven circulation, we derive a theoretical relationship between the strength of the soil moisture-induced circulation and the soil moisture. The soil moisture-induced circulation can be understood using the analogue of a sea breeze (20), wherein density gradients between the atmosphere over land and over sea generate a shallow circulation, the strength of which can be estimated using density current theory (29). In our simulation, the contrast in soil moisture between precipitating and nonprecipitating regions affects the properties of the boundary layer air via changes in the surface sensible heat flux and generates the requested density contrast.

We thus start by relating the sensible heat flux F_{SH} to the soil moisture ϕ using the linearized version of the surface energy budget equation

$$Q = F_{SH}(\phi)\left[1 + \frac{L_v}{c_p}\frac{r_a}{r_a + r_s(\phi)}\frac{\partial q_s}{\partial T}\right] + \rho L_v \frac{q_s[1 - RH]}{r_a + r_s(\phi)} \qquad [1]$$

with r_s as given in Eq. **5**. Q is the surface net radiation, q_s the saturation-specific humidity in the lowest layer of the atmosphere, T the temperature, RH the relative humidity, and ρ the density (1 kg·m^{-3}), as well as the thermodynamic constants $L_v = 2.5 \times 10^6$ J·kg^{-1} and $c_p = 1{,}006$ J·kg^{-1}·K^{-1}. To solve Eq. **1** we assume that the surface and atmospheric states are known in the limiting case of r_s approaching 0 s·m^{-1}, i.e., in the precipitating region (see *SI Appendix*, section 1 for more detail and *SI Appendix*, Table S1 for a list of all of the simulation values used to solve Eqs. **1**–**4**). Fig. 4*A* confirms that, despite assuming atmospheric parameters that do not vary with ϕ in Eq. **1**, the theoretical curve is able to reproduce the simulated dependency of the sensible heat flux upon soil moisture.

A change in F_{SH} leads to a corresponding response of the boundary layer properties. The latter response is computed using

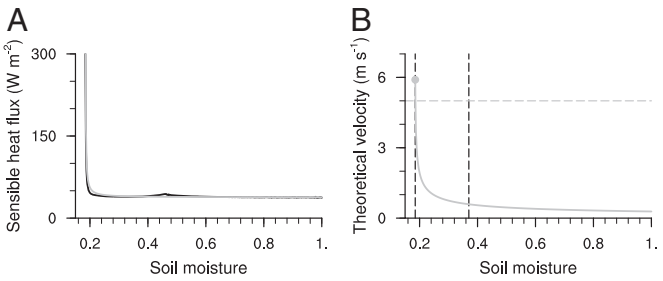

Fig. 4. (*A*) Daytime averaged values (6–18 local time) of sensible heat flux binned by soil moisture (black) together with their theoretical estimate (gray line, Eq. **1**) as well as (*B*) theoretical velocity c of the soil moisture-induced circulation (Eq. **4**) as a function of soil moisture. The two dashed black lines in *B* are field capacity (0.37) and permanent wilting point (0.185). Circle shows the simulated soil moisture value 1 d before the precipitation starts falling in the desiccated region.

the bulk theory of a convective boundary layer of height h deepening into a layer of uniform stratification Γ (30),

$$\theta_v(\phi) = \theta_v^0 + \Gamma h(\phi) \quad [2]$$

$$h(\phi) = \sqrt{\frac{2}{\Gamma}\left(\frac{F_{SH}(\phi)}{\rho c_p}\right)t}, \quad [3]$$

where we use θ_v as a density measure and neglect the small contribution of the latent heat flux in Eq. **3**. Ensuing perturbations in θ_v, if strong enough, spin up a circulation with velocity c given by (29, 31)

$$c(\phi) = k\sqrt{\frac{gH\,\Delta\theta_v(\phi)}{\theta_v^0}} = k\sqrt{\frac{gH\,[\theta_v(\phi) - \theta_v(r_s = 0)]}{\theta_v^0}} \quad [4]$$

with k constant, H the depth of the circulation, and $g = 9.81\ \mathrm{m\cdot s^{-2}}$. The resulting velocity is plotted in Fig. 4*B*. Note that a similar curve can be obtained by using an equilibrium framework, as in ref. 32 (*SI Appendix*, section 1 and Fig. S1*B*). The velocity of the radiatively driven circulation rarely reaches $5\ \mathrm{m\cdot s^{-1}}$ so that a value of c larger than this should be sufficient to offset the radiatively driven circulation. From Fig. 4*B*, it is evident that this requires a complete drying of the soil: When the plants wilt, the rain comes.

This finding is a direct consequence of the strength of the radiatively driven circulation combined with the very nonlinear shape of the velocity curve c set by the chosen resistance function r_s (compare Fig. 4 and *SI Appendix*, Fig. S1*A*). Changes in our simulation setup do not influence this basic response (*SI Appendix*, sections 1 and 2). Although prescribing larger r_s values, as used in the European Centre for Medium-Range Weather Forecasts (ECMWF) model, yields an earlier homogenization of the precipitation, the soil still needs to lose 85% of its water availability to do so (*SI Appendix*, Fig. S2). More importantly, Fig. 4 indicates that at least at the permanent wilting point, all soils will be able to attract precipitation. This is so because shutting down evaporation produces a very strong temperature perturbation. The skin temperature is by up to 7 K warmer over the desiccated region. This is much stronger than what can be obtained from boundary layer cooling (*SI Appendix*, section 1 and Fig. S3), cloud radiative effects, or over sea surfaces.

The fact that the evaporation is always fully controlled by the atmosphere, except when approaching the permanent wilting point (Fig. 4*A*), also prevents a direct control of soil moisture on the precipitating region. This control would conspire to maintain the precipitation in the precipitating region and lead to a reduction of the precipitating area α as the soil moisture and consequently the latent heat flux averaged over the precipitating area F_{LH}^{p} increase. However, even when using a larger initial r_s, no evidence of such an effect is found. As a first working hypothesis, we may assume that the domain-mean precipitation P, which is controlled by the atmospheric energy budget, does not change significantly as F_{LH}^{p} changes. This constraint implies that a reduction in α following from an increase in F_{LH}^{p} has to be compensated by a decrease in the latent heat flux averaged over the nonprecipitating area F_{LH}^{np}, as $F_{LH}^{p} < F_{LH}^{np}$ in RCE simulations due to the strong drying of the near-surface air in the nonprecipitating region. But this latter fact also implies that, as α decreases, F_{LH}^{np} tends to increase rather than decrease, in contradiction with the previous requirement. If instead we assume that the change in F_{LH}^{np} remains negligible as F_{LH}^{p} increases, then a reduction in α requires that the precipitation averaged over the precipitating region P^p increases faster than F_{LH}^{p}. This follows from the constraint that $\alpha = \frac{P}{P^p} = \frac{\alpha F_{LH}^{p} + (1-\alpha)F_{LH}^{np}}{P^p}$ in equilibrium. At least from a direct soil moisture–precipitation feedback perspective, where an increase in latent heat flux leads to a corresponding increase in precipitation, this is not possible either. Hence, although a direct control of soil moisture on the precipitating area cannot be excluded, the above arguments might explain why such a control is difficult to realize.

The Width of Intertropical Convergence Zones

Our simulation results, despite their robustness across various model configurations, remain confined to a grossly simplified ansatz to the real world. Some of the neglected processes, in particular shear, are known to cause convective organization. Here, we explore the extent to which the developed ideas might help explain observations on the one hand and rationalize difficulties faced by climate models in representing the dynamics of precipitation margins over land on the other hand. We do so by exploring the interannual variability of the ITCZ margin over northern Africa.

The northward extent of the summer rains over Africa has received considerable attention due to its importance for Sahelian rainfall (33, 34). The interannual variability in Sahelian rainfall is primarily associated with SST variability with some contribution from land–atmosphere interactions. To investigate whether the northward extent of the ITCZ might correlate with the dryness of northern African soils, we define the ITCZ margin for one particular year as the 95th percentile of the latitudes where the 2-d zonally averaged precipitation falls below $0.1\ \mathrm{mm\cdot h^{-1}}$. We average over a 2-d time period and take the 95th percentile to reduce misidentification of the ITCZ location due to sporadic convective systems that propagate out of the main ITCZ region. The dryness of the continent is determined based on observed photosynthetically active radiation (*Materials and Methods*).

Fig. 5 shows the mean location of the ITCZ together with its northward margin vs. the dryness of northern Africa (red *Inset*). The latter suggests that in years when a larger portion of northern Africa is at the permanent wilting point, the ITCZ penetrates farther inland. Although this result is consistent with the line of thinking encouraged by the RCE simulations, such effects will in practice be difficult to separate from related but different drivers of circulation (35). But it might have important consequences for the representation of precipitation margins in climate models.

Climate models with convective parameterization have difficulties in reproducing the width of the ITCZ and its northward extent, a well-known pitfall in particular for Holocene simulations (36, 37). It has already been demonstrated that climate models do not reproduce the preferential triggering of convection over the Sahel by soil moisture-induced circulation, where the soil moisture patchiness results from previous convective

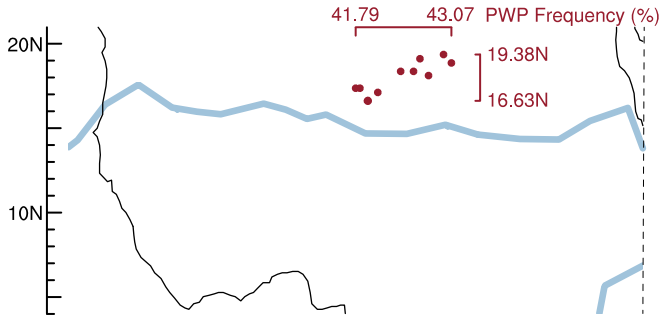

Fig. 5. Mean location of the ITCZ over northern Africa in summer 2006 (blue contour) together with location of the northern ITCZ margin for the years 2003–2012 (red circles) as a function of the continental dryness. The latter is computed as the frequency of occurrence (in percentage) of the permanent wilting point over northern Africa: western coast to 40° E (dashed line), Equator to 25° N, and over the time period February–May (monthly outputs) before the ITCZ reaches its summer position. The mean location of the ITCZ corresponds to the 2 mm·d^{-1} smoothed precipitation contour.

systems falling over the Sahel (11). Also, convective parameterizations tend to strongly distort the representation of surface-induced circulation (38), and the strength of surface gradients is muted by the limited resolution of large-scale models. It is thus unlikely to expect that the semiarid regions can attract some of the precipitation from the more humid region, as happens in the RCE simulation, which leads us to speculate that explicitly resolving the convection and the interplay between nonprecipitating and precipitating regions may solve the problem of the monsoon propagation during the Holocene.

Summary

Letting radiation, convection, and soil moisture interact with each other in an initially homogeneous land–atmosphere system indicates that the fundamental role of soil moisture is to bring precipitation from the precipitating to the nonprecipitating region. Against initial expectations, we find no significant evidence of a positive feedback between soil moisture and precipitation that would conspire to maintain the precipitation in the precipitating region, as do interactions between radiation and convection.

Our results emphasize the important role of the interactions between nonprecipitating (arid) regions and large-scale organized regions of precipitation in determining the spatial distribution of precipitation (Fig. 6): The atmosphere organizes the convection in large-scale features and maintains a circulation with surface flow from the nonprecipitating to the precipitating region. This circulation develops from the distinct radiative heating profiles of the two regions. Once the soil dries out, however, the shutdown of evaporation and the ensuing strong gradient in sensible heat flux spin up a shallow circulation with surface flow from the precipitating to the nonprecipitating region. This circulation alters the direction of the radiatively driven circulation and brings back the precipitation. As the precipitation replenishes the soil moisture, the surface forcing disappears, but the precipitation persists until other areas of the domain become dry enough to reorganize the circulation and steal the precipitation. The radiatively driven circulation requires the dry boundary layer to be colder. To offset this, sufficient surface warming is needed. We use theories developed to understand density current propagation, the transient growth of the boundary layer, and the surface energy budget, to understand and quantify the requested amount of drying. We find hints in observations that a larger extent of soil moisture conditions at the permanent wilting point over northern Africa indeed leads to a stronger inland penetration of the ITCZ.

Our study focused on one key difference between land and ocean, i.e., the fact that the land can dry out. Analyzing the effect of their distinct heat capacity (*SI Appendix*, section 2) confirms that the ability of the land to influence precipitation depends strongly on its ability to generate circulations. Here, the very nonlinear response of evaporation to soil moisture, which is expected to be mediated by other surface properties that we did not consider, has a decisive effect. Shutting down evaporation is very efficient at generating strong circulations, circulations that are much stronger than what can be obtained through radiative effects or SST gradients. Also, the circulations are strong enough to promote the development of convection in an otherwise unfavorable atmospheric environment. Once the surface winds converge in the nonprecipitating region, precipitation comes in only about 3 d, whereas more than 50 d of continuous moistening by latent heat flux does not lead to the production of any significant precipitation.

Materials and Methods

Our simulation setup is akin to past studies of radiative convective equilibrium (e.g., ref. 4) albeit including a simple representation of the land surface. We use the University of California Large-Eddy Simulation (UCLA-LES) model integrated at a convection-permitting resolution of 3 km, on a domain of 576 km^2 with a model top at 27 km, and integrated for 150 d. The insolation is horizontally homogeneous but includes a diurnal cycle, and there is no background wind and no rotation. Further details on the model setup are given in ref. 39; see their experiment U50D. The only difference from U50D is the inclusion of an interactive soil moisture.

The coupling to the land surface happens via a skin layer. The energy budget equation is solved for the skin layer assuming a heat capacity of 20,000 J·kg^{-1}·m^{-2} (equation 1 in ref. 40) and neglecting the ground heat flux. The latter contribution can be safely neglected on timescales longer than 1 d. The surface fluxes are computed as in equations 2 and 3 of ref. 40. For the computation of the latent heat flux, a soil moisture resistance r_s is added in series to the atmospheric resistance r_a. We use a classical resistance formulation given by

$$r_s(\phi) = r_{s,fc}\frac{\phi_{fc} - \phi_{pwp}}{\phi - \phi_{pwp}} \quad [5]$$

with ϕ soil moisture, ϕ_{fc} field capacity (0.37), ϕ_{pwp} permanent wilting point (0.185), and $r_{s,fc}$ soil moisture resistance at field capacity (1 s·m^{-1}). To predict the soil moisture, we use a simple bucket soil model where soil moisture is increased by precipitation and decreased by evaporation. We assume a soil depth of 1 m. The initial soil moisture is set to 0.475, corresponding to the porosity of the chosen soil type. The soil type corresponds to loamy clay, a frequent soil type in the Consortium for Small-scale Modeling (COSMO) model (table 11.1 in ref. 41). We neglect runoff formation. Including runoff would have forced us to put back the water in some way in the system to ensure conservation of water, which is not a straightforward choice. As a consequence of this choice, the soil becomes oversaturated in the precipitating region. This is akin to the formation of a water pond at the surface, as

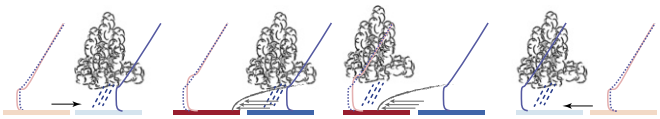

Fig. 6. Schematic representation of the main phases summarizing the interactions between organized convection, soil moisture, and their associated shallow circulations. Black arrow shows radiatively driven circulation, and gray arrows show soil moisture-induced circulation. Blue (red) shows positive (negative) soil moisture anomaly: the darker the color, the stronger the anomaly. The vertical lines are indicative of the potential temperature profiles.

happens on a rainy day. The sensitivity of our results to the chosen properties of the land surface is investigated in *SI Appendix*.

For observations, we use precipitation from the Tropical Rainfall Measuring Mission Multisatellite Precipitation Analysis (TMPA), soil moisture from the Advanced Microwave Scanning Radiometer - Earth Observing Satellite (AMSR-E), and the fraction of absorbed photosynthetically active radiation (FAPAR) provided by the Copernicus Global Land Service over the time period 2003–2012. Resolutions are 0.25° for TMPA and AMSRE and 0.5° for FAPAR. As the permanent wilting point theoretically represents the point at which the plants begin to wilt and manifests itself by a drastic decrease of the radiation absorbed by plants, we combine the observations of soil moisture and of photosynthetically active radiation to determine the permanent wilting point. This is done by plotting the fraction of absorbed photosynthetically active radiation as a function of soil moisture and graphically determining the inflexion point of the curve. To do so the data are averaged monthly and stratified by plant cover class to account for differing vegetation characteristics.

Primary data and scripts used in the analysis that may be useful in reproducing the authors' work are archived by the Max Planck Institute for Meteorology and can be obtained by contacting publications@mpimet.mpg.de.

ACKNOWLEDGMENTS. We acknowledge use of the supercomputer facilities at the Deutsches Klimarechenzentrum as well as discussion with Juan Pedro Mellado. We also acknowledge the very valuable reviews by Tim Cronin and an anonymous reviewer, which both helped clarify our manuscript and strengthen our main conclusions. This study was supported by the Max Planck Society for the Advancement of Science and the Hans Ertel Centre for Weather Research. The Hans Ertel Centre for Weather Research is a research network of Universities, Research Institutes, and the Deutscher Wetterdienst funded by the Federal Ministry of Transport, Building, and Urban Development.

1. Manabe S, Strickler RF (1964) Thermal equilibrium of the atmosphere with a convective adjustment. *J Atmos Sci* 20:361–385.
2. Popke D, Stevens B, Voigt A (2013) Climate and climate change in a radiative-convective equilibrium version of ECHAM6. *J Adv Model Earth Syst* 5:1–14.
3. Tompkins AM, Craig GC (1998) Radiative-convective equilibrium in a three-dimensional cloud-ensemble model. *Q J R Meteorol Soc* 124:2073–2097.
4. Bretherton CS, Blossey PN, Khairoutdinov M (2005) An energy-balance analysis of deep convective self-aggregation above uniform SST. *J Atmos Sci* 62:4273–4292.
5. Wing AA, Emanuel K (2013) Physical mechanisms controlling self-aggregation of convection in idealized numerical modeling simulations. *J Adv Model Earth Syst* 6:59–74.
6. Muller CJ, Held IM (2012) Detailed investigation of the self-aggregation of convection in cloud-resolving simulations. *J Atmos Sci* 69:2551–2565.
7. Holloway CE, et al. (2017) Observing convective aggregation. *Surv Geophys* 38:1199–1236.
8. Tobin I, Bony S, Roca R (2012) Observational evidence for relationships between the degree of aggregation of deep convection, water vapor, surface fluxes and radiation. *J Clim* 25:6885–6904.
9. Satoh M, Aramaki K, Sawada M (2016) Structure of tropical convective systems in aquaplanet experiments: Radiative-convective equilibrium versus the earth-like experiment. *SOLA* 12:220–224.
10. Cronin TW, Wing AA (2017) Clouds, circulation, and climate sensitivity in a radiative-convective equilibrium channel model. *J Adv Model Earth Syst* 9:2883–2905.
11. Taylor CM, et al. (2013) Modeling soil moisture-precipitation feedback in the Sahel: Importance of spatial scale versus convective parameterization. *Geophys Res Lett* 40:6213–6218.
12. Hohenegger C, Brockhaus P, Bretherton CS, Schär C (2009) The soil moisture-precipitation feedback in simulations with explicit and parameterized convection. *J Clim* 22:5003–5020.
13. Orlowsky B, Seneviratne SI (2010) Statistical analyses of land-atmosphere feedbacks and their possible pitfalls. *J Clim* 23:3918–3932.
14. Guillod BP, Orlowsky B, Miralles DG, Teuling AJ, Seneviratne SI (2015) Reconciling spatial and temporal soil moisture effects on afternoon rainfall. *Nat Commun* 6:6443.
15. Cronin TW, Emanuel KA, Molnar P (2015) Island precipitation enhancement and the diurnal cycle in radiative-convective equilibrium. *J Adv Model Earth Syst* 5:843–849.
16. Becker T, Stevens B (2014) Climate and climate sensitivity to changing CO2 on an idealized land planet. *J Adv Model Earth Syst* 6:1205–1223.
17. Rochetin N, Lintner BR, Findell KL, Sobel AH, Gentine P (2014) Radiative-convective equilibrium over a land surface. *J Atmos Sci* 27:8611–8629.
18. Findell KL, Eltahir EAB (2003) Atmospheric controls on soil moisture-boundary layer interactions. Part I: Framework development. *J Hydrometeorol* 4:552–569.
19. Gentine P, Holtslag AAM, D'Andrea F, Ek M (2013) Surface and atmospheric controls on the onset of moist convection over land. *J Hydrometeorol* 14:1443–1462.
20. Segal M, Arritt R (1992) Nonclassical mesoscale circulations caused by surface sensible heat-flux gradients. *Bull Am Meteorol Soc* 73:1593–1604.
21. Pielke RA (2001) Influence of the spatial distribution of vegetation and soils on the prediction of cumulus convective rainfall. *Rev Geophys* 39:151–177.
22. Taylor CM, et al. (2011) Frequency of Sahelian storm initiation enhanced over mesoscale soil-moisture patterns. *Nat Geosci* 4:430–433.
23. Taylor CM, de Jeu RAM, Guichard F, Harris PP, Dorigo WA (2012) Afternoon rain more likely over drier soils. *Nature* 489:423–426.
24. Froidevaux P, Schlemmer L, Schmidli J, Langhans W, Schär C (2014) Influence of the background wind on the local soil moisture-precipitation feedback. *J Atmos Sci* 71:782–799.
25. Naumann AK, Stevens B, Hohenegger C, Mellado JP (2017) A conceptual model of a shallow circulation induced by prescribed low-level radiative cooling. *J Atmos Sci* 74:3129–3144.
26. Hohenegger C, Stevens B (2013) Preconditioning deep convection with cumulus congestus. *J Atmos Sci* 70:448–464.
27. Kumar VV, Protat A, Jakob C, May PT (2014) On the atmospheric regulation of the growth of moderate to deep cumulonimbus in a tropical environment. *J Atmos Sci* 71:1105–1120.
28. Bergemann M, Jakob C (2016) How important is tropospheric humidity for coastal rainfall in the tropics? *Geophys Res Lett* 43:5860–5868.
29. Simpson JE (1969) A comparison between laboratory and atmospheric density currents. *Q J R Meteorol Soc* 95:758–765.
30. Tennekes H (1973) A model for the dynamics of the inversion above a convective boundary layer. *J Atmos Sci* 30:558–567.
31. Seitter KL (1986) A numerical study of atmospheric density current motion including the effects of condensation. *J Atmos Sci* 43:3068–3076.
32. Betts AK (2000) Idealized model for equilibrium boundary layer over land. *J Hydrometeorol* 1:507–523.
33. Nicholson SE (2009) A revised picture of the structure of the "monsoon" and land ITCZ over West Africa. *Clim Dyn* 32:1155–1171.
34. Giannini A, Saravanan R, Chang P (2003) Oceanic forcing of Sahel rainfall on interannual to interdecadal time scales. *Science* 302:1027–1030.
35. Biasutti M, Sobel AH, Camargo SJ (2009) The role of the Sahara low in summertime Sahel rainfall variability and change in the CMIP3 models. *J Clim* 22:5755–5771.
36. Joussaume S, et al. (1999) Monsoon changes for 6000 years ago: Results of 18 simulations from the paleoclimate modeling intercomparison project (PMIP). *Geophys Res Lett* 26:859–862.
37. Claussen M, Dallmeyer A, Bader J (2017) Theory and modeling of the African humid period and the green Sahara. *Oxford Research Encyclopedia of Climate Science* (Oxford Univ Press, New York), pp 1–39.
38. Hohenegger C, Schlemmer L, Silvers L (2015) Coupling of convection and circulation at various resolutions. *Tellus A* 67:26678.
39. Hohenegger C, Stevens B (2016) Coupled radiative convective equilibrium simulations with explicit and parameterized convection. *J Adv Model Earth Syst* 8:1468–1482.
40. Rieck M, Hohenegger C, van Heerwaarden CC (2014) The influence of land surface heterogeneities on cloud size development. *Mon Weather Rev* 142:3830–3846.
41. Doms G, et al. (2011) A description of the nonhydrostatic regional COSMO model Part II: Physical parameterization. Available at www.cosmo-model.org/content/model/documentation/core/cosmoPhysParamtr.pdf. Accessed April 2018.